

# Experimental Analysis of the Relationship between Flow Velocities and Sediment Transport in a Laboratory Channel Featuring a Lateral Bifurcation and Sand Bed

Darío Calderón<sup>1</sup>, Khaled Hamad-Mohamed<sup>2</sup>, Jorge Escobar-Ortiz<sup>3\*</sup>

**Abstract** — This experimental study investigates the relationship between flow velocities and sediment transport in a laboratory flume featuring a 90° lateral bifurcation with a mobile sediment bed composed of medium sand ( $D_{50} = 1.06$  mm). The experiment was conducted at the Center for Research and Studies in Water Resources Engineering of the National Polytechnic School (CIERHI-EPN) using a scaled, fixed-geometry open-channel model under subcritical flow conditions with a constant discharge of 40 l/s. The objective is to establish empirical, experimentally validated correlations between flow structures and sediment dynamics in bifurcated channels. Instantaneous flow velocities were recorded at over 180 points using an Acoustic Doppler Velocimeter (ADV), and topographic measurements of the sediment bed were used to quantify scour and deposition. A total of 43.3 l of sand was scoured (with maximum depth of 15.01 cm), 8.0 l was redeposited (up to 8.49 cm thick), and 35.3 l was transported beyond the mobile bed. Results indicate that flow is predominantly one-dimensional in the upstream channel, while the bifurcation induces complex three-dimensional velocity components ( $V_x$ ,  $V_y$ ,  $V_z$ ) associated with shear layers, vortex formation, and sediment redistribution. Compared to previous studies that focused on fixed beds or numerical simulations, this research provides high-resolution, experimental evidence of the link between secondary flow structures and sediment transport patterns under mobile-bed conditions. The findings contribute to improved predictive capabilities for morphodynamic behavior in natural bifurcations and support the development of more efficient sediment control and hydraulic design strategies.

**Keywords:** bifurcation, Acoustic Doppler Velocimeter (ADV), sediment transport, open-channel flow.

\* Authors acknowledge the support provided by Escuela Politécnica Nacional. Corresponding author: [jorge.escobaro@epn.edu.ec](mailto:jorge.escobaro@epn.edu.ec)

1. Darío Calderón Author is with the Centro de Investigaciones y Estudios de Ingeniería de los Recursos Hídricos & Departamento de Ingeniería Civil y Ambiental at Escuela Politécnica Nacional, Quito 170517, Ecuador. E-mail: [dario.calderon@epn.edu.ec](mailto:dario.calderon@epn.edu.ec), ORCID number <https://orcid.org/0000-0003-2171-5809>
2. Khaled Hamad-Mohamed Author is with the Centro de Investigaciones y Estudios de Ingeniería de los Recursos Hídricos & Departamento de Ingeniería Civil y Ambiental at Escuela Politécnica Nacional, Quito 170517, Ecuador. E-mail: [khaled.hamad@epn.edu.ec](mailto:khaled.hamad@epn.edu.ec), ORCID number <https://orcid.org/0000-0001-9365-9602>
3. Jorge Escobar-Ortiz Author is with the Centro de Investigaciones y Estudios de Ingeniería de los Recursos Hídricos & Departamento de Ingeniería Civil y Ambiental at Escuela Politécnica Nacional, Quito 170517, Ecuador. E-mail: [jorge.escobaro@epn.edu.ec](mailto:jorge.escobaro@epn.edu.ec), ORCID number <https://orcid.org/0000-0003-3862-1657>

DOI: <https://doi.org/10.29019/enfoqueute.1150>

Associate Editor: Marcelo Mosquera

**Resumen** — Este estudio experimental investiga la relación entre las velocidades del flujo y el transporte de sedimentos en un canal de laboratorio con una bifurcación lateral de 90°, equipado con un lecho móvil compuesto por arena media ( $D_{50} = 1.06$  mm). El experimento se realizó en el Centro de Investigaciones y Estudios en Ingeniería de los Recursos Hídricos de la Escuela Politécnica Nacional (CIERHI-EPN), utilizando un modelo físico de canal abierto con geometría fija, operado en condiciones de flujo subcrítico y con un caudal constante de 40 l/s. El objetivo es establecer correlaciones empíricas validadas experimentalmente entre las estructuras del flujo y la dinámica del sedimento en canales bifurcados. Se registraron velocidades instantáneas del flujo en más de 180 puntos mediante un velocímetro acústico Doppler (ADV), y se realizaron mediciones topográficas del lecho para cuantificar la socavación y la sedimentación. En total, se socavaron 43.3 l de arena (con una profundidad máxima de 15.01 cm), se redepositaron 8.0 l (con espesores de hasta 8.49 cm), y se transportaron 35.3 l más allá del lecho móvil. Los resultados indican que el flujo es predominantemente unidimensional en el canal de aproximación, mientras que la bifurcación induce componentes tridimensionales del flujo ( $V_x$ ,  $V_y$ ,  $V_z$ ), asociados a capas de corte, formación de vórtices y redistribución de sedimentos. En comparación con estudios previos que se enfocan en lechos fijos o simulaciones numéricas, esta investigación aporta evidencia experimental de alta resolución sobre la relación entre estructuras de flujo secundario y patrones de transporte de sedimentos en condiciones de lecho móvil. Los hallazgos contribuyen a mejorar la capacidad predictiva del comportamiento morfodinámico en bifurcaciones naturales y respaldan el desarrollo de estrategias más eficientes para el control de sedimentos y el diseño hidráulico.

**Palabras Clave:** bifurcación, velocímetro acústico Doppler (ADV), transporte de sedimentos, flujo en canal abierto.

## I. INTRODUCTION

RIVER bifurcations, also known as diffluences, are critical geomorphological features where a single channel divides into two downstream branches, influencing flow partitioning, sediment transport, and channel stability. These junctions are fundamental in river deltas, alluvial fans, braided rivers, avulsions, anastomosing rivers, meanders or sinuous curves or bends in rivers, floodplains and meanders rectification and engineered waterway networks [1], where their stability dictates the long-

term morphological evolution of riverine environments [2]. Mismanagement of sediment transport at bifurcations can lead to excessive deposition, erosion, or channel abandonment, which are crucial factors for hydraulic infrastructure design [3].

Among the key hydrodynamic processes governing bifurcated flows is the Bulle effect—a three-dimensional phenomenon in which near-bed, low-momentum flow and sediment are preferentially diverted into one branch of the bifurcation, often the lateral or secondary channel. This effect, driven by counter-rotating secondary vortices, causes an asymmetrical distribution of sediment load and contributes to scour in the main branch and deposition near the secondary channel entrance [4], [5]. As such, the Bulle effect introduces a nonlinear sediment partitioning mechanism that cannot be captured by depth-averaged models, highlighting the need for detailed experimental and three-dimensional analysis in bifurcation studies.

Despite their significance, bifurcations have historically received less attention compared to confluences. However, recent experimental, numerical, and field-based studies have refined our understanding of bifurcation dynamics. Laboratory experiments have demonstrated that bifurcation asymmetry—especially at large divergence angles—tends to promote channel abandonment through sediment plugging, reinforcing previous theories on the self-strangulation of secondary branches [6]. These studies, while insightful, have focused primarily on simplified configurations or idealized bifurcation angles under controlled conditions. In parallel, high-resolution numerical models have examined the influence of downstream boundary conditions and branch lengths on bifurcation stability [7].

However, such simulations are typically conducted under fixed-bed assumptions and symmetrical layouts, which limits their ability to replicate morphodynamic processes associated with mobile-bed conditions and sharp-angle bifurcations. The present study complements these efforts by experimentally investigating an asymmetrical bifurcation with a mobile sediment bed under controlled flow conditions, enabling direct observation of sediment dynamics and quantification of erosion–deposition patterns in geometries not fully addressed in prior work.

Numerical simulations have significantly contributed to understanding and predicting sediment partitioning at river bifurcations. For instance, [8] developed a one-dimensional morphodynamic model that incorporates erodible banks and local channel width adjustments. Their findings demonstrated that gravel-bed bifurcations naturally evolve toward asymmetric stable configurations, where one branch consistently captures most of the flow and sediment. Similarly, [9] implemented a field-validated framework for predicting water and sediment fluxes across delta bifurcations under varying discharge conditions. By integrating graph-based models and nodal relations derived from channel geometry and hydraulics, they achieved accurate partitioning estimates even in data-sparse environments. These studies underline the capacity of 1D and 3D models to reveal how sediment loads and planform variables control morphological evolution and long-term avulsion or stabilization patterns.

In contrast, simulations and field studies incorporating tidal influences highlight different stabilization mechanisms. [10] investigated two highly asymmetric, tide-affected bifurcations in the Kapuas River delta. Their findings revealed that neither

transverse bed slopes nor inlet steps were sufficient to stabilize bifurcations dominated by suspended sediment transport. Instead, bed material sorting and the geometry of the side branches—particularly inlet width and depth—played critical roles in determining sediment division. These observations suggest that tidal dynamics may reduce branch dominance by dampening flow gradients, thus promoting morphological resilience in systems where fluvial and tidal forcings interact.

Field-scale research has reinforced the practical relevance of computational findings by validating them under real-world conditions. For example, [11] developed a quasi-two-dimensional model for braided gravel-bed rivers that revealed how small changes in the upstream Shields parameter can trigger shifts between symmetric and asymmetric bifurcation equilibria. However, their model assumes fixed banks and simplified loop geometries, limiting its applicability to natural systems with variable planform and mobile boundaries.

In a complementary approach, [12] implemented a physically-based moving boundary model to simulate sediment-laden inflows into lakes and reservoirs. Their results demonstrated how delta progradation and bottomset mud deposition are tightly coupled to turbidity current dynamics, but the scenarios assume stratified standing water and do not include fluvial bifurcation under open-channel flow. These examples illustrate how numerical modeling has advanced our understanding of bifurcation dynamics and deltaic evolution, while also highlighting the need for controlled experimental data to validate assumptions and extend their applicability to non-idealized channel systems.

Advances in bifurcation research have practical implications for river engineering and sediment management. Hydraulic interventions such as dredging and artificial bifurcation stabilization can trigger systemic morphological adjustments, including the formation of wedge-shaped sand plugs, channel abandonment, and significant redistribution of bed material across distributaries. [6] demonstrated experimentally that high diversion angles promote sediment deposition at the bifurcation's outer bank, leading to self-reinforcing sand plug growth and eventual disconnection of the diverted branch. Similarly, [10] showed that in tidally influenced bifurcations, interventions modifying the inlet geometry or flow distribution may alter the sediment-to-water division ratio. Such changes can destabilize the sediment balance and accelerate or inhibit branch siltation, depending on the interplay between bed material sorting, secondary flows, and tidal modulation. These findings underscore the necessity of adaptive sediment management strategies that integrate hydrodynamic and morphodynamic feedbacks to prevent unintended channel evolution and maintain long-term stability.

Emerging methodologies, such as high-resolution satellite imaging and computational fluid dynamics (CFD) simulations, are transforming bifurcation stability studies. Remote sensing techniques using Landsat imagery have facilitated long-term monitoring of bifurcation evolution, while advanced modeling platforms like Delft3D have provided new insights into the impacts of climate change and human interventions on bifurcation dynamics [7]. However, such numerical models have typically been applied under idealized conditions involving symmetrical geometries and fixed beds. As a result, they do not fully captu-

re the morphodynamic complexity of acute-angle bifurcations with mobile sediment beds. The present experimental study addresses this gap by investigating, under controlled laboratory conditions, how flow redistribution affects sediment transport and local bed evolution in an asymmetrical bifurcation with a mobile granular bed.

However, despite these advances, a detailed understanding of how three-dimensional flow structures interact with sediment dynamics in sharp-angle lateral bifurcations under mobile bed conditions remains limited. Most existing studies either focus on fixed-bed scenarios, large-scale river systems with complex boundary conditions, or numerical predictions that require experimental validation. There is still a need for controlled laboratory experiments that can isolate the effects of velocity gradients, vortex shapes, and flow partitioning on localized scour and sediment deposition. Addressing this gap is crucial for improving sediment management strategies and informing the design of stable bifurcation systems.

This research aims to bridge existing knowledge gaps by conducting controlled laboratory experiments in a bifurcated channel with a mobile sediment bed. Using high-precision Acoustic Doppler Velocimetry (ADV), this study investigates the correlation between velocity distribution, sediment transport, and bifurcation stability. The experimental findings enable the identification of quantifiable relationships between hydrodynamic patterns and morphodynamic responses, offering a foundation for improving conceptual understanding and informing the calibration and validation of future numerical or field-based predictive models. These insights also support practical sediment management strategies in hydraulic engineering, with direct applications to river stabilization, flood mitigation, and waterway navigation management.

## II. MATERIALS AND METHODS

### A. Conceptual Framework, Experimental Design, and Benchmarking with Previous Studies

This study was initiated through a comprehensive review of the existing literature and the conceptual design of a physical modeling facility at the Center for Research and Studies in Water Resources Engineering (CIERHI) of the National Polytechnic School (EPN). The experimental platform was developed within a laboratory equipped with a closed-loop water recirculation system capable of delivering up to 100 l/s, constrained by pump power and head losses. The working area, approximately 200 m<sup>2</sup>, was limited by the presence of adjacent experimental setups. In addition, a total of 800 kg (480 l) of non-cohesive sediment was available for experimental use.

These physical and operational constraints defined the configuration of the facility, including the geometry of the flume, slope selection, sediment retention and collection systems, and the positioning of the water intake and measurement units. The system incorporated complementary structures—such as dissipation tanks, sediment traps, scaffolding, and walkways—to ensure safe operation and facilitate accurate data acquisition. Preliminary hydraulic calculations were carried out to define the

channel length, width, depth, and slope required to generate the desired sediment transport regime under subcritical conditions.

The sediment used consisted of uniform quartz sand with a median diameter  $D_{50} = 1.06$  mm, selected for its well-documented behavior in experimental studies of sediment mobility and morphodynamics. This grain size falls within the range commonly employed in laboratory bifurcation studies [13] and ensures fully turbulent flow, bedload-dominated transport, and rapid morphological adjustment, enabling the identification of scour and deposition processes within practical timeframes. The uniformity of the material minimizes grain-size sorting effects and supports the reproducibility of bedforms, while avoiding cohesion or clustering that might interfere with sediment transport dynamics.

The geometric configuration of the experimental facility was established based on hydraulic design criteria and sediment transport considerations. The height of the mobile bed was defined through the estimation of local scour using five different analytical methods commonly applied in bridge foundation design [14]. Among these, the method proposed by [15] yielded the most critical depth ( $h = 0.32$  m), and a conservative design thickness of  $h = 0.30$  m was adopted for construction. The channel width was set to  $b = 0.60$  m to allow high-resolution velocity profiling across five transverse sections spaced 10 cm apart using an Acoustic Doppler Velocimeter (ADV). The length of the approach channel ( $L = 4.0$  m) was experimentally calibrated to ensure fully developed flow before the bifurcation, while the downstream main channel ( $L = 2.0$  m) and the secondary branch ( $L = 0.94$  m) were designed to accommodate the sand bed, flow redistribution, and sediment transport beyond the bifurcation node.

The selected discharge of  $Q = 40$  l/s and the normal flow depth above the bed ( $d_0 = 0.24$  m) were determined iteratively to ensure that the dimensionless shear stress remained below the critical Shields parameter for incipient motion and that the resulting critical slope was lower than the channel slope ( $S = 0.1\%$ ). The sidewall height ( $H = 0.60$  m) was chosen to safely contain both the mobile bed and the constant water depth, maintaining a freeboard of 0.06 m. The resulting design velocity near the bifurcation junction was approximately  $U_0 = 0.28$  m/s.

The experimental sediment consisted of non-cohesive quartz sand with a median grain size  $D_{50} = 1.06$  mm, selected for its proven suitability in morphodynamic flume studies. Previous experiments on mobile-bed bifurcations have employed similar particle sizes ranging from 0.5 mm to 1.1 mm [13], [16], [17], which ensure bedload-dominated transport under turbulent conditions and allow for rapid morphological response without cohesive interference. Furthermore, the adopted geometric parameters—including a 0.30 m sand thickness, 0.60 m flume width, and 4.0 m approach length—align with established experimental configurations in the literature and are consistent with validated setups for bifurcation flow-sediment interaction studies.

Previous research has demonstrated the effectiveness of physical models in analyzing sediment–flow interactions at bifurcations. [18] studied sediment transport in 90° diversions, confirming the importance of controlled laboratory conditions. However, this study was based on a fixed-bed experimental setup

with relatively short test durations (45-75 minutes), which limited the observation of long-term morphological evolution and bed feedback processes. [6] showed that bifurcation angles significantly influence sediment deposition and channel evolution, underscoring the need for precise geometric control in physical experiments. Nevertheless, these experiments were focused on idealized geometries and did not address configurations with sharp angles and fully mobile sediment beds, nor did they quantify the uncertainty associated with measured flow velocities.

To address these limitations, the present study introduces a mobile-bed laboratory setup with over 180 high-resolution velocity measurements, using the SonTek FlowTracker2 ADV. The instrument provides velocity accuracy within 1 % of the measured value per second, with uncertainty analysis grounded in Interpolated Variance Estimator (IVE) and ISO-748 methods [19]. Moreover, quality control is ensured through parameters such as Signal-to-Noise Ratio ( $\text{SNR} \geq 10$  dB) and velocity standard error ( $< 0.01$  m/s), as specified in the manufacturer's guidelines [20], [21]. This methodology enhances the reliability of the experimental data and addresses gaps in precision and representativeness noted in earlier studies.

### B. Experimental Flume Configuration and Hydraulic Setup

Based on the hydraulic and sediment transport design considerations, the physical modeling facility was constructed at the Center for Research and Studies in Water Resources Engineering (CIERHI), located in Quito, Ecuador. The experimental flume consists of a prismatic, transparent acrylic channel measuring 4.0 m in length, 0.60 m in width and height, with a longitudinal slope of 0.1 %. Transparent acrylic walls were selected due to their smoothness and high optical clarity, which are ideal for flow visualization and accurate ADV measurements in laboratory conditions. A 90° lateral bifurcation branches off the main channel into a secondary arm measuring 2.0 m in length, with identical cross-sectional dimensions and slope.

The bifurcation zone was designed to simulate natural sediment–flow interactions and includes a mobile sediment bed with a uniform thickness of 0.30 m, extending 1.70 m along the main channel and 0.93 m along the secondary branch. The bed was filled with well-sorted quartz sand characterized by a median grain size  $D_{50} = 1.06$  mm, with  $D_{16} = 0.85$  mm,  $D_{84} = 1.40$  mm, a specific weight of  $1660$  kg/m<sup>3</sup>, a uniformity coefficient  $C_u = 1.49$ , and a curvature coefficient  $C_c = 1.03$ .

To realistically represent fluvial bifurcations under controlled laboratory conditions, the channel geometry was deliberately configured with a sharp divergence angle ( $\sim 90^\circ$ ) and uniform rectangular cross-sections in both branches. This planform asymmetry is frequently encountered in natural systems such as deltas and distributary networks, where it promotes the development of flow separation zones, secondary vortices, and sediment plug formation. The flat bed and constant slope further enable precise control over sediment mobilization and redistribution. This configuration allows for the reproduction and monitoring of key morphodynamic processes—such as branch flow redistribution, vortex-driven transport, and localized scour—that are essential to the stability and evolution of natural and engineered bifurcations.

Flow control at the downstream end of the secondary channel is achieved using a vertically adjustable gate positioned 0.132 m from the channel top (0.468 m from the bottom), regulating flow to maintain a water depth of 0.24 m above the sand bed. The calculated recirculating flow rate was 40 l/s. Fig. 1A) shows the perspective view of the setup, while Fig. 1. B) details the sand bed and its key dimensions.

### C. Preliminary Calibration and Bed Adjustment for Equilibrium Conditions

Preliminary testing involved verifying watertightness, expected flow patterns, and initial sediment behavior. It was found that the original geometry of the bed did not allow an adequate development of sediment transport phenomena, especially in the secondary channel, whose short length prevented the sedimentation of sand in the area downstream of the main mound that was being formed. Therefore, the distribution of the sand bed was adjusted with the purpose of locating it in the areas of greatest occurrence of sediment transport phenomena, shortening its length in the main channel by 0.30 m and extending it in the secondary channel by 0.30 m, but maintaining its width and height, resulting in the final configuration shown in Fig. 1. B).

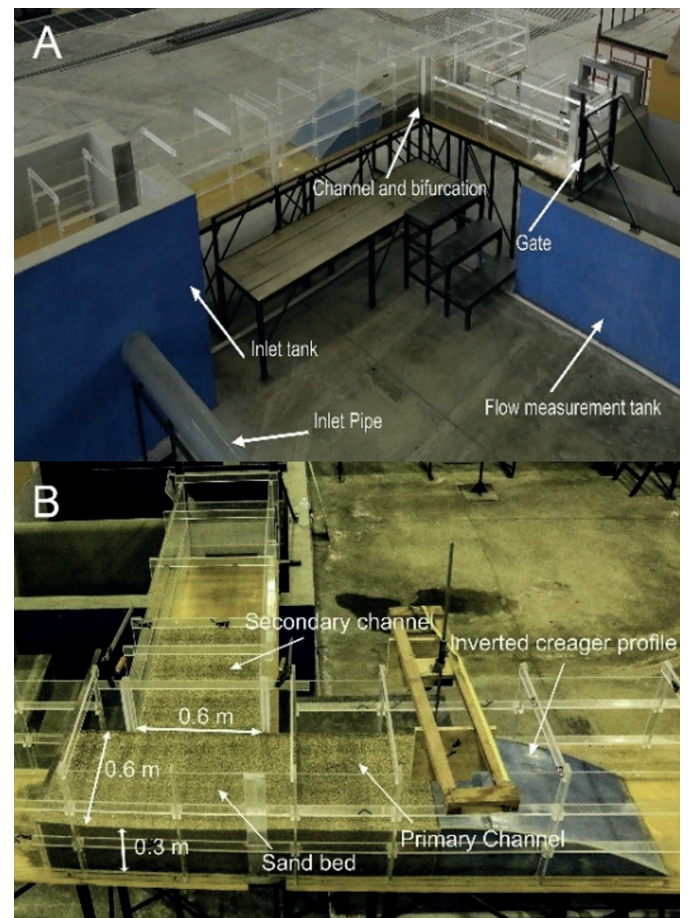


Fig. 1. Experimental facility A) Perspective view. B) Sand bed and its main dimensions.

Boundary conditions were defined to remain constant throughout testing (flow rate  $Q = 40$  l/s, water depth  $d_0 = 0.24$  m, chan-

nel width  $b = 0.60$  m and channel slope  $S = 0.1$  %), the average velocity calculated for the main approach channel is  $U_0 = 0.28$  m/s, while flow velocities and sediment transport varied spatially in the area of the bifurcation, which will be further detailed below. A flow rate of 40 l/s was maintained continuously for 24 hours until a relative equilibrium between scour and deposition was reached, the criterion used to determine bed equilibrium is the absence of movement in the sediments while the water is still flowing [22] It should be emphasized that the subsequent velocity measurement was performed only after equilibrium had been reached in the sediment transport, i.e. when no more spatial variations of the bed were recorded, so that the movement of the sand particles would not affect the validity of the velocities obtained.

*D. Bathymetric Survey of the Mobile Bed and Resolution Constraints*

The topographic survey of the sand bed (bathymetry) was carried out at the bifurcation of the experimental facility. For this purpose, mobile limnimeters were used following a matrix or grid drawn every 3 cm in the X and Y directions. For both channels there are limitations on bed edge measurements, it was not possible to topographically survey the edges of the sand bed with a thickness between 1.0 and 4.5 cm due to the physical impossibility of lowering the limnimeters in these areas located next to the acrylic pieces that compose the main and secondary channels. Details of their dimensions and location are shown in Fig. 2, where the cross and normal sections at whose intersections the flow velocities were measured are also shown, as explained in the following section.

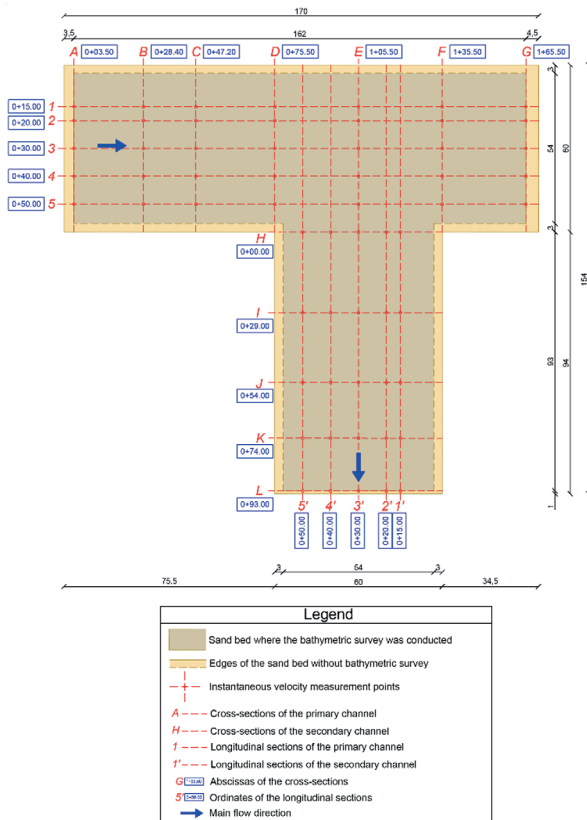


Fig. 2. Dimensions and location of the surveyed sand bed and remaining edges.

The sediment used in this study —uniform quartz sand with a median grain size of approximately 1.06 mm— is typically transported as bedload, primarily through rolling and saltation under subcritical flow conditions. Due to its relatively high settling velocity, this particle size exhibits limited suspension unless subjected to intense turbulence or near-flood conditions. The dominance of near-bed transport in such granulometric ranges justifies the use of fine-resolution bathymetric grids (3 cm × 3 cm), as most morphological changes —such as scour and deposition— occur close to the sediment–flow interface and within short spatial scales [23], [24].

Moreover, the well-sorted nature of the sediment (with a uniformity coefficient  $C_u = 1.49$ ) facilitates coherent bedform development and predictable mobilization once the Shields threshold is exceeded. In contrast to poorly sorted mixtures, uniform sediments promote synchronized particle entrainment and well-defined morphological structures such as ripples or dunes, enhancing the reproducibility and interpretability of bathymetric measurements [25], [26]. Thus, both the granulometry and the high-resolution survey strategy contribute to the robustness of the morphological data collected in this flume experiment.

*E. Three-Dimensional Velocity Measurement and Experimental Flow Characterization*

Flow directions were defined with X as the longitudinal axis, Y as transverse, and Z as vertical (Fig. 3), allowing systematic assessment of velocity components within both channels.

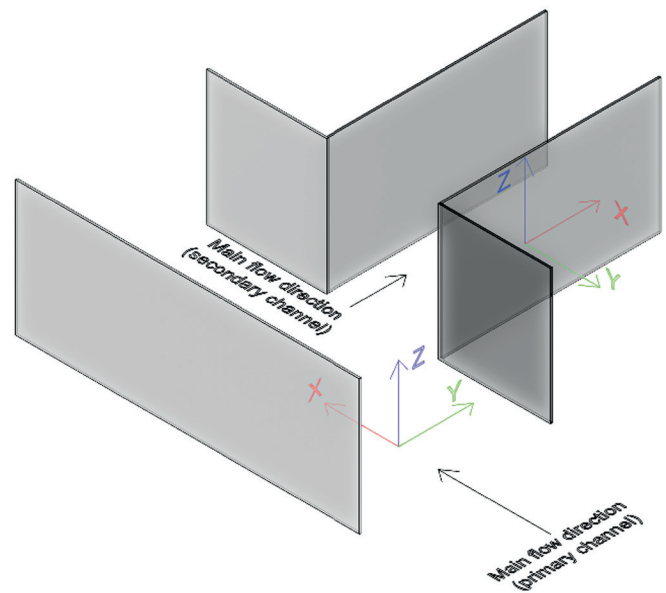


Fig. 3. Schematic of the spatial directions or components (X, Y, Z) adopted for the flow in the primary and secondary channels.

Instantaneous flow velocities were taken at more than 180 points, defined by the intersection between cross sections (YZ planes), normal (XZ planes) and longitudinal (XY planes); distributed as follows:

- By varying the abscissae X, 7 cross sections were chosen for the main channel (A, B, C, D, E, F and G) and

5 cross sections for the secondary channel (H, I, J, K and L); these were defined according to the physical space available for the location of the ADV and its support on the channels.

- By varying the Y ordinates, 5 normal sections were chosen for the main channel (1, 2, 3, 4 and 5) and 5 normal sections for the secondary channel (1', 2', 3', 4' and 5'); these were defined according to the lateral distance that the equipment must have from the solid objects for optimum performance.
- Varying the Z dimensions, 3 longitudinal sections were chosen for both channels ( $\alpha$ ,  $\beta$  and  $\gamma$ ); these were defined according to the minimum submergence and the vertical distance that the equipment must have from solid objects for optimum performance.

The distribution of the velocity measurement points is shown in the Fig. 4, Fig. 5, Fig. 6 and Fig. 7. These locations enabled a comprehensive spatial characterization of velocity fields [27] demonstrated the efficacy of ADV technology in capturing secondary flows relevant to sediment transport. [10] further validated the precision of ADV measurements in asymmetric bifurcation setups.

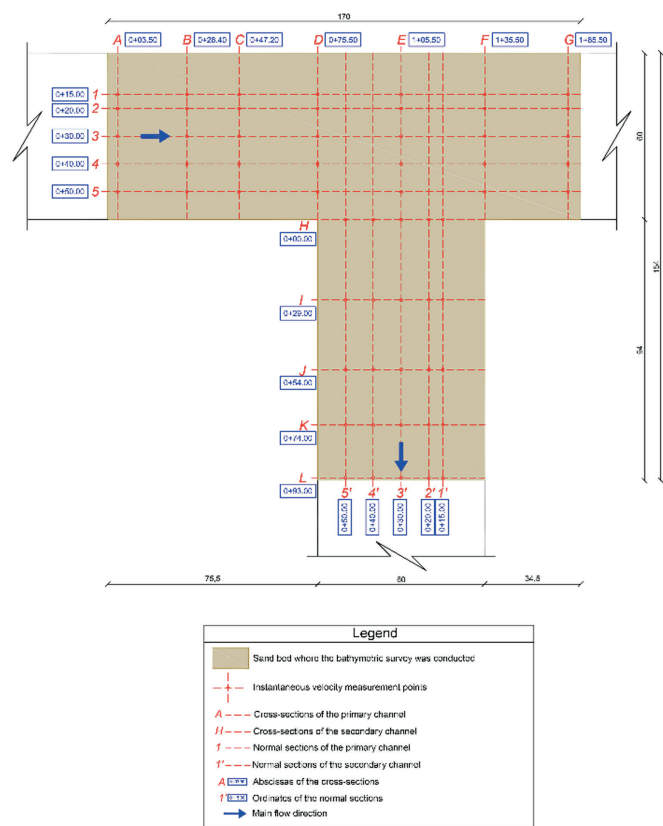


Fig. 4. Plan view diagram showing the position of the points and sections where instantaneous flow velocity measurements were taken.

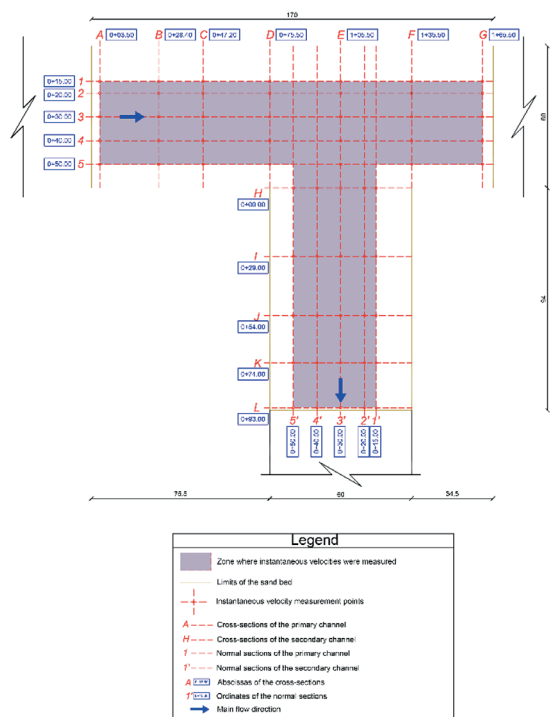


Fig. 5. Plan view diagram showing the position of the points, sections, and area where instantaneous flow velocity measurements were taken.

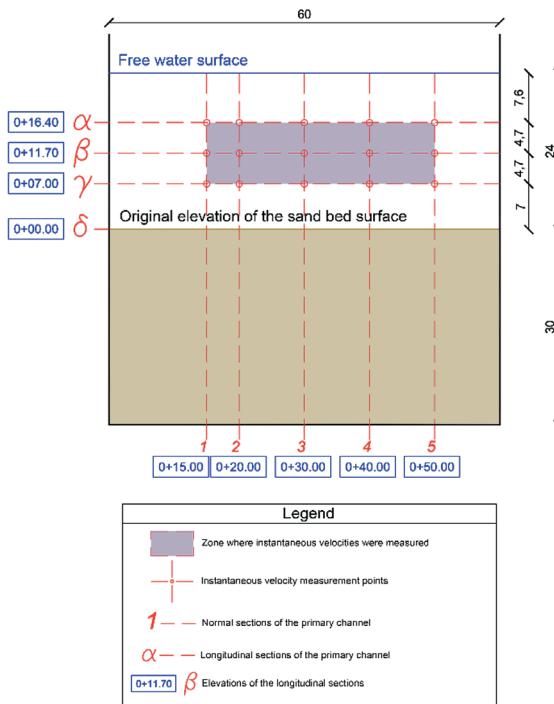
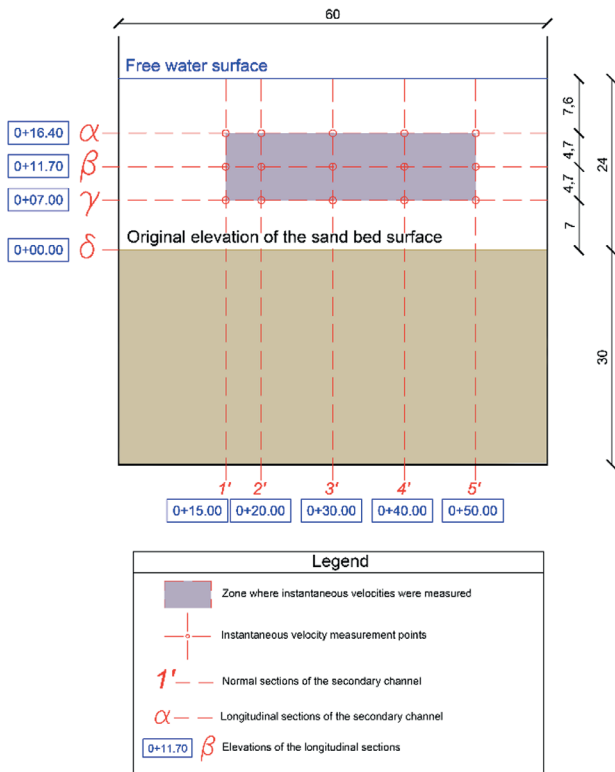


Fig. 6. Section view diagram showing the position of the points, sections, and area where instantaneous flow velocity measurements were taken in the primary channel.



**Fig. 7.** Section view diagram showing the position of the points, sections, and area where instantaneous flow velocity measurements were taken in the secondary channel.

For measuring instantaneous flow velocities, an Acoustic Doppler Velocimeter (ADV) was used, specifically the SonTek FlowTracker2, a high-technology instrument designed for three-dimensional velocity data acquisition in shallow flows [28]. Measurements were taken at over 180 locations within the bifurcation zone. At each point, velocity data were recorded for a total duration of 40 seconds, with a data output interval of 0.5 seconds, yielding 80 instantaneous velocity readings per point. The sampling rate, data filtering, and averaging were managed via the manufacturer's software suite.

The ADV probe includes a central transmitter and three acoustic receivers. To ensure data quality, care was taken to position the sampling volume at least 5 cm away from solid boundaries and above the active layer of the mobile sediment bed, avoiding signal reflection or acoustic interference. According to the manufacturer, the Signal-to-Noise Ratio (SNR) must remain between 10 and 50 dB to ensure reliable velocity measurements, and the standard deviation of the horizontal components should remain below 0.01 m/s [20]. These thresholds were verified in real time during acquisition.

Although ADVs provide high-resolution data, they can be affected by sediment suspension, signal scattering near the bed, and low flow turbulence near walls. In this study, potential disturbances were mitigated by positioning the probe well within the flow core and rejecting outlier values based on velocity standard deviation and SNR thresholds. Similar protocols have been employed in previous laboratory studies of sediment

transport in bifurcations [5], [29], where ADV performance has proven adequate under controlled conditions with mobile beds.

Studies such as those by [30] have employed similar measurement techniques to analyze velocity distribution and sediment transport in bifurcated channels, confirming the effectiveness of these methods in obtaining precise and detailed hydrodynamic data in physical models. Once the optimal conditions for proper device operation were verified, instantaneous velocities were recorded at the previously specified points as part of the experimental trials to quantitatively characterize the main hydrodynamic phenomena occurring within the setup.

To ensure that the flow conditions are representative of natural bifurcations, the experimental design was guided by dimensionless parameters commonly used in fluvial hydraulics, including Froude number, aspect ratio, and bifurcation angle. The selected slope (0.1%), sediment size ( $D_{50} \approx 1.06$  mm), and flow rates were calibrated to promote sediment mobility under turbulent flow while reproducing features such as vortex formation, flow separation, and localized scour—characteristic of bifurcating river systems. These emergent phenomena have been reported in both field and laboratory studies [5], [6], confirming the morphological and hydrodynamic similarity between the experimental setup and natural conditions.

These methodological choices align with best practices in sediment transport research and contribute to the broader understanding of hydrodynamic processes governing bifurcation stability and sediment partitioning.

### III. RESULTS AND DISCUSSION

The magnitudes of the resultant velocity vectors for the mean velocities  $V_x$ ,  $V_y$ , and  $V_z$  of the circulating flow over the sand bed in the experimental setup are graphically represented for the three longitudinal sections  $\alpha$ ,  $\beta$ , and  $\gamma$ . Analysis of the spatial velocity field in the three longitudinal sections ( $\alpha$ ,  $\beta$ , and  $\gamma$ ) provides essential data on the changes in hydrodynamic flow conditions leading to scour and sediment deposition in the bifurcation zone. Studies such as [2] and [30] confirm that the interaction between velocity fields and sediment motion is crucial in bifurcations, influencing both scouring and deposition processes.

Recent numerical studies, such as those by [8], have validated experimental observations by simulating velocity distributions and sediment behavior in bifurcations. These models confirm the existence of secondary circulations and velocity gradients that govern sediment transport, reinforcing the experimental findings of this study (Table I).

#### A. Velocity Variability in Longitudinal Sections

The graphical representation of resultant velocity vectors for mean velocities  $V_x$ ,  $V_y$ , and  $V_z$  (calculated from the average instantaneous velocities) allows for the identification of flow acceleration, deceleration, and vortex formation in each longitudinal section, which are essential in understanding sediment transport mechanisms. The spatial distribution of velocity magnitudes along the longitudinal sections reveals significant changes in flow characteristics induced by the bifurcation. The graphical representation of resultant velocity vectors—compu-

ted from the mean components  $V_x$ ,  $V_y$ , and  $V_z$  obtained from time-averaged instantaneous data—facilitates the identification of flow acceleration, deceleration, and vortex formation. These phenomena are essential to understanding sediment transport mechanisms within the bifurcation zone.

Numerical simulations by [8] predicted counter-rotating vortices forming before the bifurcation apex, a phenomenon that was also observed experimentally by [27] and [31]. These vortices influence near-bed sediment transport, leading to uneven sediment distribution between the branches.

1. LONGITUDINAL SECTION  $\alpha$

Fig. 8. illustrates the velocity distribution for longitudinal section  $\alpha$ , located at a height of 0.164 m from the original sand bed level.

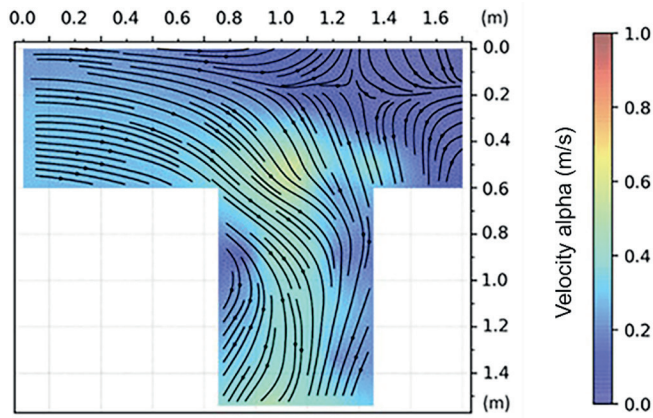


Fig. 8. Magnitudes of the resultant velocity vectors  $V$  for the mean velocities  $V_x$ ,  $V_y$ , and  $V_z$  in longitudinal section  $\alpha$  at a height of 0.164 m.

Analysis for the Primary Channel

In the primary channel, a progressive reduction in the  $V_x$  component is observed from Section A to Section F, while the  $V_y$  component increases near the bifurcation zone. This trend aligns with findings from [27], who observed similar velocity redistribution patterns in experimental bifurcations, emphasizing their crucial role in sediment transport.

The  $V_x$  velocity component exhibits values around 0.28 m/s at abscissa 0.035 m (Section A), progressively decreasing until reaching 0.00 m/s or slightly negative values at abscissa 1.655 m (Section G). The lowest  $V_x$  values for this channel are observed near the left boundary.

The  $V_y$  velocity component exhibits values around 0.00 m/s at abscissa 0.035 m (Section A), progressively increasing until reaching 0.52 m/s at abscissa 1.055 m (Section E) located at the center of the lateral bifurcation. The lowest  $V_y$  values are observed near the left boundary of the channel.

In the dead volume zone at the end of the primary channel extension, between abscissas 1.355 m (Section F) and 1.655 m (Section G), counterclockwise vertical-axis vortices form due to flow division, confirmed by the presence of both positive and negative velocity values at abscissas 1.355 m and 1.655 m. These vortices contribute to localized energy dissipation on 90° lateral diversions [31], similar to the observations made by [2] in their studies on bifurcation-induced transport mechanisms.

TABLE I  
SUMMARY OF INSTANTANEOUS VELOCITY EXTREMES AND RESULTANTS

LONGITUDINAL SECTION $\alpha$							
Main Channel							
	Normal Velocity $V_x$		Transverse Velocity $V_y$		Resultant Velocity $V$		
	Maximum	Minimum	Maximum	Minimum	Maximum	Minimum	
Value (m/s)	0.29	0	0.52	0	0.56	0	
Cross Section (Abscissa m)	A (0.035)	A (0.035)	G (1.655)	F (1.355)	E (1.055)	G (1.655)	E (1.055)
Normal Section (Ordinate m)	3 (0.30)	5 (0.50)	1 (0.05)	2 (0.20)	5 (0.50)	1 (0.15)	5 (0.50)
Secondary Channel							
	Normal Velocity $V_x$		Transverse Velocity $V_y$		Resultant Velocity $V$		
	Maximum	Minimum	Maximum	Minimum	Maximum	Minimum	
Value (m/s)	0.39	0.09	-0.44	0	0.52	0.11	
Cross Section (Abscissa m)	L (0.930)	I (0.290)	H (0.000)	K (0.740)	H (0.000)	I (0.290)	

Normal Section (Ordinate m)	2' (0.20)	5' (0.50)	3' (0.30)	3' (0.30)	3' (0.30)	5' (0.50)	
<b>LONGITUDINAL SECTION <math>\beta</math></b>							
<b>Main Channel</b>							
	<b>Normal Velocity Vx</b>		<b>Transverse Velocity Vy</b>		<b>Resultant Velocity V</b>		
	<b>Maximum</b>	<b>Minimum</b>	<b>Maximum</b>	<b>Minimum</b>	<b>Maximum</b>	<b>Minimum</b>	
Value (m/s)	0.29	0	0.49	0.01	0.53	0.03	
Cross Section (Abscissa m)	A (0.035)	A (0.035)	F (1.355)	E (1.055)	G (1.655)	E (1.055)	G (1.655)
Normal Section (Ordinate m)	3 (0.30)	5 (0.50)	4 (0.40)	5 (0.50)	1 (0.15)	5 (0.50)	1 (0.15)
<b>Secondary Channel</b>							
	<b>Normal Velocity Vx</b>		<b>Transverse Velocity Vy</b>		<b>Resultant Velocity V</b>		
	<b>Maximum</b>	<b>Minimum</b>	<b>Maximum</b>	<b>Minimum</b>	<b>Maximum</b>	<b>Minimum</b>	
Value (m/s)	0.4	0.18	-0.37	0.01	0.48	0.18	
Cross Section (Abscissa m)	L (0.930)	I (0.290)	H (0.000)	J (0.540)	I (0.290)	I (0.290)	
Normal Section (Ordinate m)	1' (0.15)	5' (0.50)	1' (0.15)	3' (0.30)	1' (0.15)	3' (0.30)	5' (0.50)
<b>LONGITUDINAL SECTION <math>\gamma</math></b>							
<b>Main Channel</b>							
	<b>Normal Velocity Vx</b>		<b>Transverse Velocity Vy</b>		<b>Resultant Velocity V</b>		
	<b>Maximum</b>	<b>Minimum</b>	<b>Maximum</b>	<b>Minimum</b>	<b>Maximum</b>	<b>Minimum</b>	
Value (m/s)	0.3	0.01	0.48	0	0.53	0.02	
Cross Section (Abscissa m)	A (0.035)	G (1.555)	E (1.055)	B (0.284)	E (1.055)	G (1.655)	
<b>LONGITUDINAL SECTION <math>\gamma</math></b>							
<b>Main Channel</b>							
Normal Section (Ordinate m)	5 (0.50)	5 (0.50)	5 (0.50)	12 (0.20)	5 (0.50)	1 (0.15)	
<b>Secondary Channel</b>							
	<b>Normal Velocity Vx</b>		<b>Transverse Velocity Vy</b>		<b>Resultant Velocity V</b>		
	<b>Maximum</b>	<b>Minimum</b>	<b>Maximum</b>	<b>Minimum</b>	<b>Maximum</b>	<b>Minimum</b>	
Value (m/s)	0.38	0.2	0.53	-0.01	0.63	0.21	
Cross Section (Abscissa m)	J (0.540)	H (0.000)	L (0.930)	J (0.540)	L (0.930)	H (0.000)	
Normal Section (Ordinate m)	4' (0.40)	1' (0.15)	5' (0.50)	1' (0.15)	5' (0.50)	1' (0.15)	

#### *Analysis for the Secondary Channel*

In the secondary channel, a progressive increase in the Vx component is observed from Section H to Section L, while the Vy component is higher near the bifurcation zone.

The Vx velocity component exhibits values around 0.21- 0.26 m/s at abscissa 0.000 m (Section H), progressively increasing until reaching 0.32 – 0.39 m/s at abscissa 0.930 m (Section L); this trend indicates flow stabilization downstream,

as the absence of additional geometric disturbances allows the flow to regain its uniform characteristics; however, variability is observed near the channel boundaries, particularly at ordinates 0.15 m (Section 1') and 0.50 m (Section 5'), with fluctuations evident at abscissas 0.29 m (Section I), 0.54 m (Section J), and 0.74 m (Section K). The lowest  $V_x$  values for this channel are observed near the right boundary.

The  $V_y$  velocity component exhibits values from 0.44 to 0.09 m/s at abscissa 0.000 m (Section H) and from 0.07 to 0.37 m/s at abscissa 0.930 m (Section L), show no clear trend. [10] A large vertical axis vortex with clockwise rotation, elongated and oval section, is identified along the X-axis; this vortex with low velocities is located on the right side of the secondary channel, in the area approximately between the intersection points of sections H and 5', H and 3', L and 5', and L and 3'. Similar vortex formations have been reported by [10], besides, studies by [6] demonstrated that vortex-induced flow changes can enhance sediment accumulation along the inner bank of a bifurcated branch, just like the results of this study.

In summary, in section  $\alpha$ , positioned 0.164 m above the original sand bed level,  $V_x$  velocity components tend to decrease at the end of the primary channel and accelerate along the secondary channel, particularly at its central ordinates. Meanwhile,  $V_y$  velocity components show higher values in the bifurcation zone of both channels, reinforcing the velocity redistribution effect of the bifurcation.

## 2. Longitudinal Section $\beta$

Fig. 9. illustrates the velocity distribution for longitudinal section  $\beta$ , located at a height of 0.117 m from the original sand bed level.

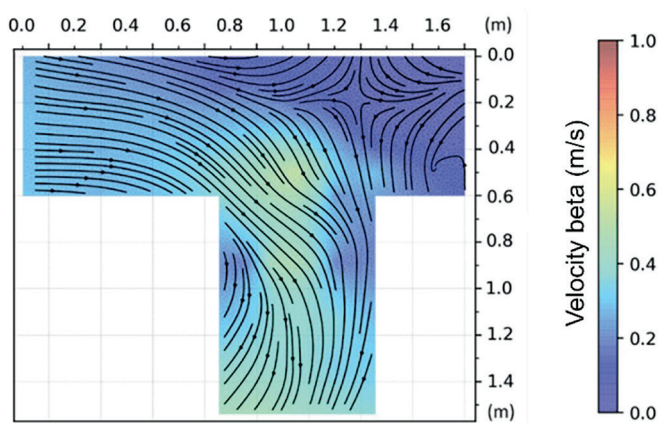


Fig. 9. Magnitudes of the resultant velocity vectors  $V$  for the mean velocities  $V_x$ ,  $V_y$ , and  $V_z$  in longitudinal section  $\beta$  at a height of 0.117 m.

### Analysis for the Primary Channel

In longitudinal section  $\beta$ , located 4.7 cm below section  $\alpha$ , the resultant velocity vectors  $V$  and their  $V_x$  and  $V_y$  components exhibit similar values, flow patterns and trends as those observed in section  $\alpha$ ; however, a notable difference is observed: in section  $\beta$ , the area occupied by vorticity zones (regions of low positive and negative velocities) is larger in the plan

view, particularly at the downstream end and along the left side of the primary channel.

The increase in the vorticity region at greater depths suggests an intensification of turbulence, which aligns with the experimental observations of [30], where turbulence intensity was found to increase with depth in bifurcated flow conditions. This behavior is crucial in sediment transport dynamics, as reported by [27], who demonstrated that secondary flow patterns at deeper layers influence the redistribution of sediment within bifurcation zones.

### Analysis for the Secondary Channel

As in the primary channel, in longitudinal section  $\beta$ , similar flow patterns and velocity trends and variations are maintained; however, a notable difference is observed: the plan-view area occupied by the low-velocity zone, which is the section of a vortex on the right side of the secondary channel, is slightly reduced. Similarly, the low-velocity area on the left side of the channel is smaller, indicating that flow velocities  $V_x$ ,  $V_y$  and vectors  $V$  are slightly higher at this elevation; it suggests more active sediment transport.

In summary, in section  $\beta$ , positioned 0.117 m above the original sand bed level, the same velocity trends observed in section  $\alpha$  are maintained, but with slightly higher velocities near the edges of both channels, except in the dead zone of the primary channel.

## 3. Longitudinal Section $\gamma$

Fig. 10 illustrates the velocity distribution for longitudinal section  $\gamma$ , located at a height of 0.070 m from the original sand bed level.

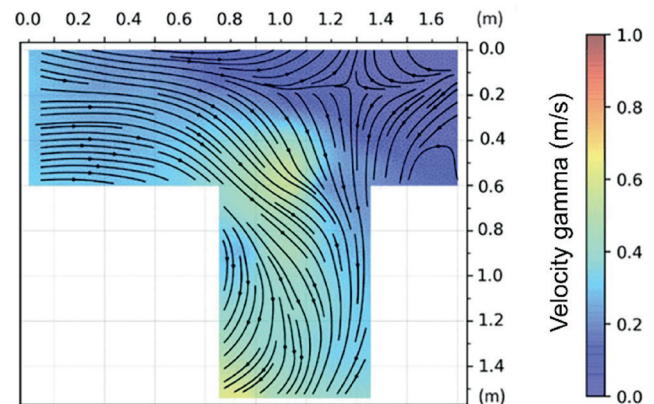


Fig. 10. Magnitudes of the resultant velocity vectors  $V$  for the mean velocities  $V_x$ ,  $V_y$ , and  $V_z$  in longitudinal section  $\gamma$  at a height of 0.070 m.

### Analysis for the Primary Channel

In longitudinal section  $\gamma$ , located 4.7 cm below section  $\beta$ , the resultant velocity vectors  $V$  and their  $V_x$  and  $V_y$  components exhibit similar values, flow patterns and trends as those observed in section  $\beta$ ; however, a notable difference is observed: in section  $\gamma$ , the area occupied by vorticity zones (regions of low positive and negative velocities) is larger in the plan view, particularly at the vicinity of the intersection between Sections F and 5. In

addition, the area of high speeds was increased at the vicinity of the intersection between Sections E and 5, being evidence of increased vorticity and turbulence in the center of the bifurcation.

*Analysis for the Secondary Channel*

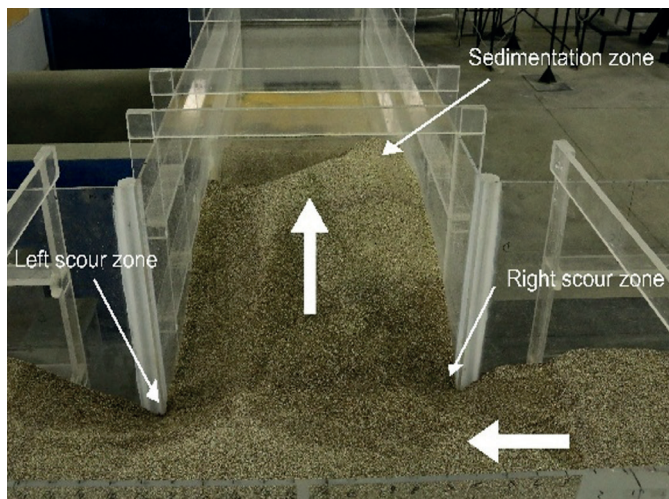
As in the primary channel, in longitudinal section  $\gamma$ , similar flow patterns and velocity trends and variations are maintained; however, a notable difference is observed: the low velocity zone corresponding to the lower section of the vertical axis vortex in the right center of the channel, has an even smaller area than in section  $\beta$ , which is indicative of its conical and inclined shape, i.e., its diameter is smaller as the flow deepens and always remains next to the channel wall. No velocity measurements were recorded exactly in the center of the vortex in the section  $\gamma$ , due to significant sediment deposition in these areas, which prevents the ADV from being positioned, given the manufacturer’s minimum distancing recommendations. The values plotted for this zone in Fig. 10. are interpolations of the data around it, therefore sedimentation does not affect the validity of the data. In addition, significant increases in velocities  $V_x$ ,  $V_y$  and  $V$  are recorded, especially in sections L and the right zone of section K.

In summary, in section  $\gamma$ , positioned 0.070 m above the original sand bed level, the same velocity trends observed in section  $\alpha$  and  $\beta$  are maintained, but with higher velocities near the edges of both channels, except in the dead zone of the primary channel. There is a vertical axis vortex in the right center of the secondary channel, it’s conical and has an inclined shape.

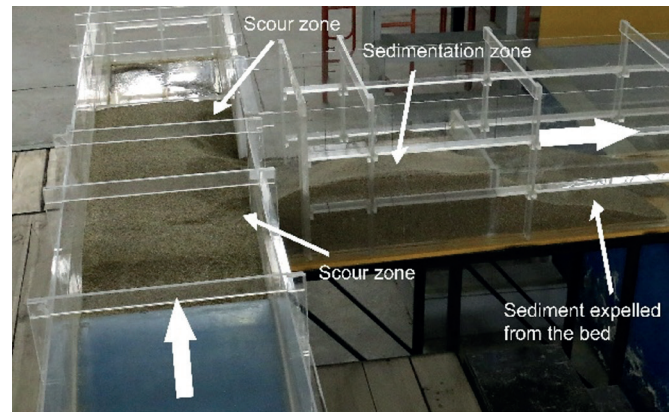
*B. Analysis of Sediment Transport Phenomena*

Fig. 11 and 12 qualitatively illustrate the sand bed formations after reaching a relative equilibrium in sediment transport within the experimental setup. These formations result in scour in some areas and sediment deposition in others, affecting both channels of the experimental installation.

Fig. 13 provides a quantitative representation of sediment transport phenomena (scour and sedimentation) through a three-dimensional depiction and topographic contour lines, where the 0.00 m level represents the original elevation of the sand bed before water flow circulation began.



**Fig. 11.** Lateral perspective view of the scour and sedimentation zones in the sand bed of the experimental setup.



**Fig. 12.** Frontal perspective view of the scour and sedimentation zones in the sand bed of the experimental setup.

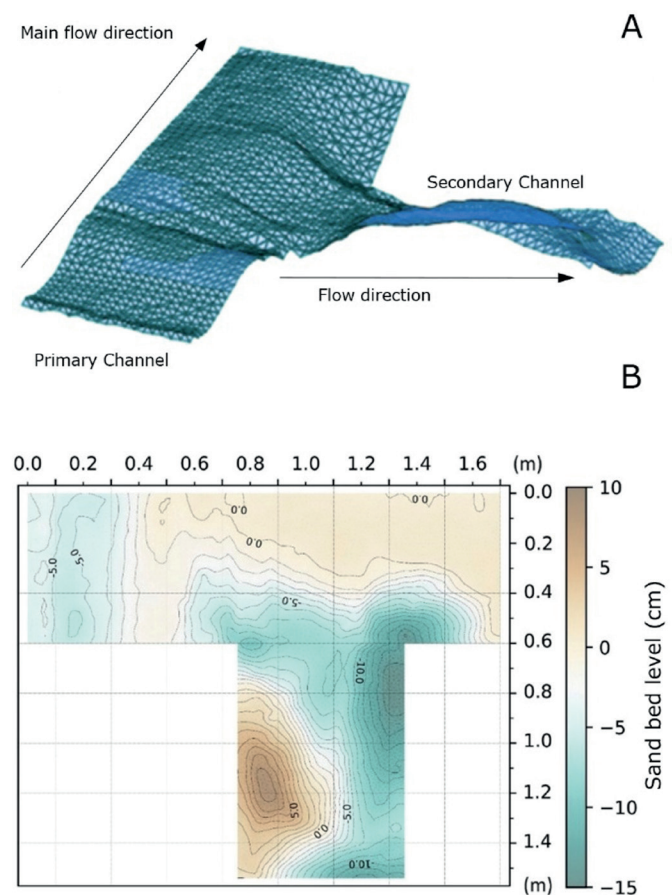


**Fig. 13.** A) Three-dimensional representation of the sand bed in the bifurcation zone after reaching a relative equilibrium in sediment transport. B) Topographic contour lines of the sand bed.

Sediment transport in the experimental setup is predominantly concentrated in the bifurcation zone, particularly along the edges connecting the two channels, specifically at the intersection of Sections D and F with Section H. The primary channel exhibits only scour processes, whereas the secondary channel experiences both scour and sedimentation phenomena.

In the primary channel, sediment transport is concentrated in Sections 4 and 5 (right zone) near the bifurcation. Conver-

sely, in Sections 1 and 2 (left zone) and further downstream of Section 3 (central zone), the sand bed remains largely undisturbed. Unrelated scour phenomena are observed in Sections A and B, occurring due to the transition from a solid, fixed bed with an inverted Creager profile to a mobile, erodible sediment bed at the entrance of the primary channel. These localized scour effects are unrelated to the bifurcation and are therefore excluded from further analysis. At abscissa 0.472 m (Section C), the original bed level is maintained, as the influence of the bifurcation on flow and sediment dynamics is still minimal in this region.

From abscissa 0.500 m onward, intense scour phenomena develop in the right and central regions of the primary channel, progressively increasing toward edge DH at abscissa 0.755 m, where a maximum scour depth of 8.71 cm is recorded. The scour extends in both X and Y directions within the secondary channel, forming an irregular pattern in the plan view.

At abscissa 1.200 m, a more intense scour phenomenon occurs, increasing towards edge FH at abscissa 1.355 m, where a maximum scour depth of 14.41 cm is reached. Similar to the previous case, this scour is concentrated around the edge, forming a distinct oval shape in the plan view, with its major axis oriented toward the secondary channel and its minor axis toward the primary channel. Beyond abscissa 1.700 m, the sediment level remains relatively undisturbed.

In the secondary channel, sediment transport affects the entire sand bed surface, with both scour and sedimentation phenomena present. These two processes are separated by the 0.0 m topographic contour line, as shown in Fig. 13B).

- In Sections 1' and 2' (left zone), only scour is observed.
- In Sections 3', 4', and 5' (center and right zone), both scour and sedimentation occur.

The most intense scour in the experimental setup is recorded at abscissa 0.000 m in the secondary channel, resulting from a combined effect of flow redirection at edges FH and DH.

- A maximum scour depth of 9.91 cm is recorded to the right at abscissa 0.000 m, ordinate 0.57 m.
- A maximum scour depth of 15.01 cm is recorded to the left at abscissa 0.120 m, ordinate 0.03 m.

These scour zones are the deepest observed within the experimental setup.

- The scour associated with edge DH extends approximately to abscissa 0.180 m (between axes H and I).
- The scour associated with edge FH extends approximately to abscissa 0.740 m (axis K).

At abscissa 0.180 m, at the far-right edge of the channel, the 0.0 m topographic contour line begins, enclosing the sediment deposition volume on the right side of the secondary channel, extending downstream to its final section at abscissa 0.930 m.

- To the left of the 0.0 m level, the entire scoured zone of the secondary channel is located, covering most of its surface in the plan view.

The oval and concentric pattern of the sediment deposition contours indicates that flow conditions favor sediment transport from the eroded bifurcation zone and its deposition downstream to the right. The sedimentation rate increases toward the centroid of the deposited volume, located at abscissa 0.540 m, ordinate 0.51 m, reaching a maximum height

of 8.49 cm. Sedimentation extends downstream up to abscissa 0.930 m (Section L).

Downstream of abscissa 0.180 m, sediment transport continues to display a left-side erosion trend and a right-side sedimentation trend, varying in intensity and shape, as illustrated in Fig. 13B).

The excess sediment transported from scoured zones, which was not deposited elsewhere within the sand bed, was expelled beyond the channel limits, primarily outside the secondary channel. The most representative sediment transport volumes recorded are:

- Total scoured (eroded) sand volume: 43.3 L
- Sedimented sand volume within the bed area: 8.0 L
- Expelled sand volume beyond the bed area: 35.3 L

These findings align with the results of [6], who demonstrated that flow division and vortex-induced scour can significantly affect sediment transport and deposition in bifurcated channel systems. Furthermore, the correlation between velocity redistribution, turbulence, and sediment deposition supports prior observations by [31] regarding the influence of bifurcations on sediment dynamics.

While the experimental results offer valuable insights into sediment behavior at bifurcations, certain constraints must be considered when extrapolating to natural river systems. The use of a uniform grain size ( $D_{50} = 1.06$  mm) does not account for selective transport, hiding effects, or differential sorting that typically occur in polydisperse sediments. Additionally, the fixed geometry of the experimental flume, although useful for controlling variables and ensuring repeatability, limits the representation of feedback mechanisms like lateral migration, bank erosion, and channel self-adjustment. These simplifications are necessary in laboratory-scale studies but should be acknowledged when interpreting morphological implications in field scenarios.

### C. Correlation for the Primary Channel

The relationship between flow velocity magnitudes and sediment transport becomes evident beyond abscissa 0.472 m (Section C), where disturbances introduced by the bifurcation significantly influence velocity redistribution and sediment dynamics.

- Scour in the DH edge zone results primarily from the 90° redirection of the main flow from the primary channel (X direction) into the secondary channel (X' direction). Additionally, flow acceleration in this zone, reaching 0.38 m/s, exceeds the mean velocity of 0.28 m/s recorded upstream (Sections A, B, and C), intensifying erosion.
- Scour at the bifurcation junction (near abscissa 1.050 m, ordinates 0.40 m and 0.50 m, Section E) is linked to turbulent, non-uniform accelerated flow, where velocity magnitudes range between 0.41 m/s and 0.56 m/s.
- Scour in the FH edge zone originates from the impact of flow streamlines against the left wall of the secondary channel, forcing an abrupt directional shift. This impact generates turbulent flow with high erosive capacity, leading to intense sediment removal.

These observed scour patterns can also be attributed to the Bulle effect, a three-dimensional flow phenomenon wherein near-bed, low-momentum fluid and sediment are preferentially redirected into the lateral branch. This occurs due to the action of counter-rotating vortices that form around the bifurcation apex, generating asymmetric velocity distributions and shear stress gradients. As a result, the diverted branch receives a disproportionate share of the sediment load, promoting deposition or sediment plugging at its entrance, while the main channel experiences enhanced scour near the node due to sediment-deficient, accelerated flow. This mechanism reinforces the erosion observed near DH and E zones, where flow redirection and secondary circulation converge [4]

Beyond abscissa 0.700 m, in the left section of the primary channel, the sand bed remains intact at 0.0 m elevation, corresponding to low flow velocities ( $<0.05$  m/s). The simultaneous presence of low velocities and absence of sediment transport is illustrated in Fig. 14.

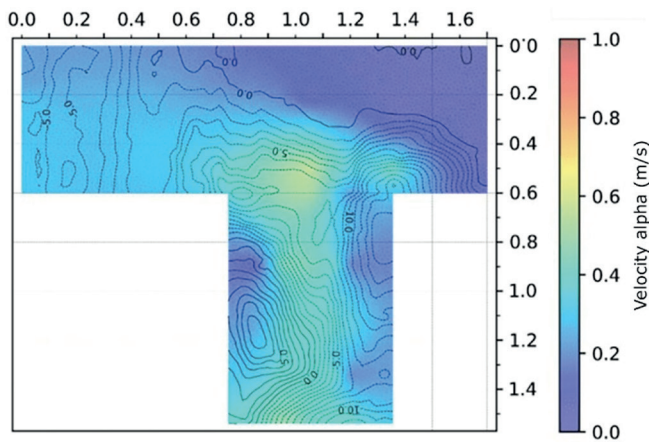


Fig. 14. Superposition of topographic contour lines on the mean velocity magnitude graph for longitudinal section  $\alpha$ .

These findings align with previous research, such as [31], which reported that scour intensity increases at bifurcation edges due to abrupt velocity vector changes and flow division.

#### D. Correlation for the Secondary Channel

At abscissa 0.000 m, along edge DH, scour intensity gradually decreases downstream until abscissa 0.200 m on the right bank of the secondary channel. Simultaneously, flow velocities reduce from 0.38 m/s to 0.15 m/s, confirming a direct correlation between velocity magnitude and scour potential.

In the central bifurcation zone (abscissa 0.000 m), higher-than-average flow velocities (0.52 m/s) correspond to scour depths between 7.6 cm and 7.9 cm.

In contrast, no direct correlation is observed between low velocities (0.17 m/s to 0.22 m/s) and scour at edge FH or downstream on the left bank of the secondary channel. Instead, sediment transport in this region is primarily driven by turbulence generated from abrupt directional changes following flow impact against the channel wall. The scour pattern extends downstream to approximately abscissa 0.700 m, mainly due to

the same turbulent phenomena, as velocities remain moderate (0.17 m/s to 0.33 m/s).

On the right side of the secondary channel, a strong correlation is observed between flow patterns and sediment transport phenomena. The vortex flow surrounds the elevations (maximum height of 8.49 cm) of the deposited sediment mass, whose centroid aligns with the vortex core, where low velocities prevail. Consequently:

- Sedimentation dominates in low-velocity zones.
- Erosion occurs in high-velocity areas.

These observations align with previous studies, such as [11], who demonstrated that vortex-induced recirculation zones play a crucial role in sediment transport dynamics. Additionally, the findings corroborate the computational results of [8], who successfully simulated secondary circulations and flow division patterns in bifurcations, validating their impact on sediment partitioning.

The flow here is dominated by secondary circulation, where lateral advection transports particles into the vortex core, while shear stress is insufficient to resuspend them. This pattern confirms that vortex-driven advection leads to sediment convergence, while reduced shear fosters stable deposition at the vortex centroid. This interpretation is consistent with the conceptual framework described by [32] and [33], where vortex-induced sorting shapes bed morphology in lateral branches.

## IV. CONCLUSIONS

This experimental study, conducted in a 60 cm-wide channel featuring a 90° lateral bifurcation and a 30 cm-thick sand bed with defined granulometry, provided significant insights into the relationships between flow velocities, flow patterns, and sediment transport phenomena. Using an Acoustic Doppler Velocimeter (ADV), instantaneous flow velocities were measured once a relative sediment transport equilibrium was achieved (state in which the sediment particles have no motion). Additionally, detailed bathymetric measurements of the sand bed allowed for a comprehensive qualitative and quantitative analysis of scour and sedimentation processes.

The design phase determined a mean flow velocity of 0.28 m/s in the primary channel, a value that closely matched the experimentally measured velocities in Section A, where streamlines corresponded to uniform flow. In this region, the  $V_x$  velocity component was dominant, while  $V_y$  and  $V_z$  components were negligible. Positive and negative values for the velocity components  $V_x$ ,  $V_y$ , and  $V_z$  were assigned according to the ADV manufacturer's predefined reference system. The highest velocities were recorded at the central junction between the channels, particularly near points E5 and H3', reaching a maximum of 0.56 m/s, while the lowest velocities were observed in the left zone at the end of the primary channel, specifically near G1, where velocities dropped to 0.00 m/s, forming a dead volume zone.

Scour phenomena were concentrated in the bifurcation zone, primarily along edges DH (depth up to 9.91 cm) and FH (depth up to 15.01 cm). These scour processes resulted from turbulence induced by the redirection of flow from the primary to

the secondary channel, as well as impact forces against the left wall of the secondary channel. In zone DH, a direct correlation was observed between high velocities (0.38 m/s to 0.52 m/s) and scour depth, whereas in zone FH, moderate velocities (0.22 m/s to 0.41 m/s) were recorded; however, scour was primarily attributed to turbulent flow effects, rather than velocity magnitude alone.

On the right side of the secondary channel, a strong correlation was found between flow patterns and sediment transport. The vortex flow surrounded the elevations of the deposited sediment mass (maximum height of 8.49 cm), whose centroid coincided with the vertical axis vortex core, where low velocities (0.11 m/s to 0.24 m/s) prevailed. Consequently, sedimentation was dominant in low-velocity zones, while erosion was prevalent in high-velocity areas. In the central junction, an evident correlation was found between higher-than-average flow velocities (0.52 m/s) and scour depths of 7.6 cm to 7.9 cm. In the primary channel, up to abscissa 0.472 m, the  $V_x$  velocity component remained predominant and relatively constant. However, downstream, the bifurcation altered velocity magnitudes and directions, increasing the significance of the  $V_y$  component, while the  $V_z$  component remained less pronounced.  $V_x$  velocities decreased toward the end of the primary channel, whereas acceleration was observed in the secondary channel, especially at central ordinates. Meanwhile,  $V_y$  components peaked near the bifurcation in both channels.

Scour in the primary channel occurred only near the bifurcation, whereas in the secondary channel, both scour and sedimentation were observed throughout the entire sand bed surface. Beyond abscissa 0.700 m, in the left zone of the primary channel, low velocities ( $< 0.05$  m/s) were recorded, correlating with the absence of sediment transport phenomena. The total eroded sand volume was 43.3 L, of which 8.0 L was redeposited within the sand bed, and 35.3 L was transported beyond the sand bed limits, primarily downstream in the secondary channel.

The quality of instantaneous velocity measurements obtained with the ADV was verified using the SNR controller. Across all measured points, SNR values remained within the recommended range of 10 dB to 50 dB. Velocity measurement points were carefully selected following ADV manufacturer guidelines, ensuring proper submergence, clearance from solid objects, and data integrity. Among the longitudinal sections  $\alpha$ ,  $\beta$ , and  $\gamma$ , flow patterns and velocity vector distributions remained consistent, with only minor variations in the plan-view size of dominant structures.  $V_z$  velocity components were detected only in regions with sediment transport, showing an upward direction in sedimentation zones and downward direction in scour zones.

Counterclockwise-rotating vertical-axis vortices developed in the dead volume of the primary channel extension (between Sections F and G). These vortices formed due to the physical constraint that prevented water from continuing downstream, forcing the flow to recirculate within the dead volume. A continuous exchange of low-discharge flow was observed between the bifurcation zone and the dead volume, with water entering near F5 and exiting near F1.

The findings of this study contribute to the understanding of sediment transport dynamics in bifurcated channels,

highlighting the influence of velocity redistribution, turbulence, vortex formation, and bifurcation-induced scour. These results provide insights applicable to the design of hydraulic structures, particularly in sediment control, flood management, and channel stability.

Among the limitations of this experimental study, the most important are related to the inputs and space available in the experimental area of CIERHI; the amount of sand with specific granulometry for this study was limited (800 kg or 480 L), which made it necessary to limit the area of the sediment bed and locate it specifically in the areas where sediment transport phenomena were more intense; If there had been more space and a larger amount of sand with specific granulometry, the dimensions of the channels and the sediment bed would have been larger, which would surely have allowed us to gather more information and experimental data.

Another limitation of the experimental study was derived from the restrictions of the ADV manufacturer, related to the submergence and minimum distances that must be respected for the measurements of instantaneous velocities to be correct; this resulted in the area where experimental data were recorded being limited and having a distance of 7 cm with respect to the bed and 10 to 15 cm with respect to the channel walls, leaving areas whose velocities could not be recorded. A final limitation is related to obtaining bathymetry using limnimeters, whose supports prevented the reading of the edges of the sediment bed, between 1.0 and 4.5 cm.

It is recommended that future research should attempt to overcome the limitations of the present experimental study, so that the sediment bed is wide enough to cover the entire bottom of both channels; in addition, the use of state-of-the-art laboratory equipment is recommended to allow the measurement of velocity profiles in areas even closer to the bed and walls of the channels. It is also recommended that similar studies be conducted, varying design and operational parameters such as flow rate, water depth on the bed, angle of the bifurcation, sediment size and distribution (grain size), and sediment type, in order to broaden the results and determine the sensitivity of changes in each of the variables considered.

## REFERENCES

- [1] C. De Hidráulica, D. María, J. E. Ayala, M. I. José and A. González Verdugo, "Estudio de bifurcaciones en ríos. Informe Final," Jiutepec, Morelos, 2015.
- [2] R. N. Szupiany *et al.*, "Flow fields, bed shear stresses, and suspended bed sediment dynamics in bifurcations of a large river," *Water Resour Res*, vol. 48, no. 11, 2012. <https://doi.org/10.1029/2011WR011677>
- [3] R. E. Thomas *et al.*, "An experimental study of discharge partitioning and flow structure at symmetrical bifurcations," *Earth Surf Process Landf*, vol. 36, no. 15, pp. 2069-2082, Dec. 2011. <https://doi.org/10.1002/esp.2231>
- [4] I. Ibrahim, S. Legori Ibrahim and S. Khan, "Flow structures in dividing open channels: A review," in *IOP Conference Series: Earth and Environmental Science*, Institute of Physics Publishing, Feb. 2020. <https://doi.org/10.1088/1755-1315/437/1/012008>
- [5] A. Momplot, G. Lipeme Kouyi, E. Mignot, N. Rivière and J. L. Bertrand-Krajewski, "Typology of the flow structures in dividing open channel flows," *Journal of Hydraulic Research*, vol. 55, no. 1, pp. 63-71, Jan. 2017. <https://doi.org/10.1080/00221686.2016.1212409>
- [6] L. Szewczyk, J. L. Grimaud and I. Cojan, "Experimental evidence for bifurcation angles control on abandoned channel fill geometry," *Earth*

- Surface Dynamics*, vol. 8, no. 2, pp. 275-288, Apr. 2020. <https://doi.org/10.5194/esurf-8-275-2020>
- [7] L. Durante, M. Bolla Pittaluga, G. Porcile, and N. Tambroni, "Downstream Control on the Stability of River Bifurcations," *J Geophys Res Earth Surf*, vol. 129, no. 10, Oct. 2024. <https://doi.org/10.1029/2023JF007548>
- [8] S. Miori, R. Repetto and M. Tubino, "A one-dimensional model of bifurcations in gravel bed channels with erodible banks," *Water Resour Res*, vol. 42, no. 11, Nov. 2006. <https://doi.org/10.1029/2006WR004863>
- [9] T. Y. Dong *et al.*, "Predicting water and sediment partitioning in a delta 1 channel network under varying discharge conditions," 2020. <https://doi.org/10.1029/2020WR027199>.
- [10] K. Kästner and A. J. F. Hoitink, "Flow and suspended sediment division at two highly asymmetric bifurcations in a river delta: implications for channel stability," *J Geophys Res Earth Surf*, vol. 124, no. 10, pp. 2358-2380, Oct. 2019. <https://doi.org/10.1029/2018JF004994>
- [11] M. Bolla Pittaluga, R. Repetto and M. Tubino, "Channel bifurcation in braided rivers: Equilibrium configurations and stability," *Water Resour Res*, vol. 39, no. 3, 2003. <https://doi.org/10.1029/2001WR001112>
- [12] S. Kostic and G. Parker, "Formation des deltas de sable et de boue dans les lacs et les réservoirs. Iière Partie. Théorie et modélisation numérique," *Journal of Hydraulic Research*, vol. 41, no. 2, pp. 127-140, 2003, <https://doi.org/10.1080/00221680309499956>
- [13] B. Federici and C. Paola, "Dynamics of channel bifurcations in non-cohesive sediments," *Water Resour Res*, vol. 39, no. 6, 2003. <https://doi.org/10.1029/2002WR001434>
- [14] M. E. Guevara Álvarez, *Socavación en puentes: evaluación, instrumentación y cálculo*. Popayán, Colombia: Editorial Universidad del Cauca, 2021.
- [15] E. M. Laursen and A. Toch, "Scour around bridge piers and abutments, HR-30 and Iowa Highway Research" in cooperation with THI IOWA State Highway Commission and The Bureau of Public Roads, 1956.
- [16] M. Naghavi, M. Mohammadi, G. Mahtabi and J. Abraham, "Experimental assessment of velocity and bed shear stress in the main channel of a meandering compound channel with one-sided blocks in floodplain," *J Hydrol (Amst)*, vol. 617, p. 129073, Feb. 2023. <https://doi.org/10.1016/j.jhydrol.2023.129073>
- [17] L. Malik and M. A. Matin, "Experimental study on flow and sediment distribution at off-take channel," *International Journal of Environmental Science and Development*, vol. 12, no. 2, pp. 35-41, 2021. <https://doi.org/10.18178/ijesd.2021.12.2.1315>
- [18] A. H. Casas and A. Bateman Pinzón, "Experimental and theoretical analysis of flow and sediment transport in 90-degree fluvial diversions," 2013. Universitat Politècnica de Catalunya.
- [19] B. Standard and B. ISO, "Hydrometry—Measurement of liquid flow in open channels using current-meters or floats," 2007, ISO.
- [20] SonTek – a Xylem brand. (2019). *FlowTracker2 User's Manual* (Version 1.6). Xylem Inc. [https://www.geotechenv.com/Manuals/SonTek\\_Manuals/sontek\\_flowtracker2\\_manual.pdf](https://www.geotechenv.com/Manuals/SonTek_Manuals/sontek_flowtracker2_manual.pdf)
- [21] S. J. McLelland and A. P. Nicholas, "A new method for evaluating errors in high-frequency ADV measurements," 2000.
- [22] T. Kostić, Y. Ren and S. Theobald, "3D-CFD analysis of bedload transport in channel bifurcations," *Journal of Hydroinformatics*, vol. 26, no. 2, pp. 480-493, Feb. 2024. <https://doi.org/10.2166/hydro.2024.175>
- [23] M. H. García, *Sedimentation Engineering*. Reston, VA: American Society of Civil Engineers, 2008. <https://doi.org/10.1061/9780784408148>
- [24] P. R. Wilcock and S. T. Kenworthy, "A two-fraction model for the transport of sand/gravel mixtures," *Water Resour Res*, vol. 38, no. 10, Oct. 2002. <https://doi.org/10.1029/2001WR000684>
- [25] L. C. van Rijn, "Sediment Transport, Part II: Suspended Load Transport," *Journal of Hydraulic Engineering*, vol. 110, no. 11, pp. 1613-1641, Nov. 1984. [https://doi.org/10.1061/\(ASCE\)0733-9429\(1984\)110:11\(1613\)](https://doi.org/10.1061/(ASCE)0733-9429(1984)110:11(1613))
- [26] P. R. Wilcock, "Critical shear stress of natural sediments," *Journal of Hydraulic Engineering*, vol. 119, no. 4, pp. 491-505, Apr. 1993. [https://doi.org/10.1061/\(ASCE\)0733-9429\(1993\)119:4\(491\)](https://doi.org/10.1061/(ASCE)0733-9429(1993)119:4(491))
- [27] W. A. Marra, D. R. Parsons, M. G. Kleinhans, G. M. Keevil and R. E. Thomas, "Near-bed and surface flow division patterns in experimental river bifurcations," *Water Resour Res*, vol. 50, no. 2, pp. 1506-1530, 2014. <https://doi.org/10.1002/2013WR014215>
- [28] K. Hamad Mohamed, "Submerged vanes turbulence: experimental analysis," 2015.
- [29] Y. Wang and A. Jacob Odgaard, "Flow control with vorticity," *Journal of Hydraulic Research*, vol. 31, no. 4, pp. 549-562, 1993.
- [30] A. Das, B. C. Barman and N. Nandi, "On some aspects of flow characteristics of the bifurcated channel – An experimental approach," *ISH Journal of Hydraulic Engineering*, vol. 29, no. 2, pp. 147-153, Mar. 2023. <https://doi.org/10.1080/09715010.2022.2042862>.
- [31] A. Herrero, A. Bateman and V. Medina, "Water flow and sediment transport in a 90° channel diversion: An experimental study," *Journal of Hydraulic Research*, vol. 53, no. 2, pp. 253-263, Mar. 2015. <https://doi.org/10.1080/00221686.2014.989457>
- [32] I. Nezu and H. Nakagawa, *Turbulence in Open-Channel Flows*. Routledge, 2017. <https://doi.org/10.1201/9780203734902>
- [33] J. L. Best, "Flow dynamics at river channel confluences: implications for sediment transport and bed morphology," in *Recent Developments in Fluvial Sedimentology*, SEPM (Society for Sedimentary Geology), 1987, pp. 27-35. <https://doi.org/10.2110/pec.87.39.0027>